Polymer Brushes at Curved Surfaces

C. M. Wijmans* and E. B. Zhulina†

Department of Physical and Colloid Chemistry, Wageningen Agricultural University, Dreijenplein 6, 6703 HB Wageningen, The Netherlands

Received May 18, 1993; Revised Manuscript Received October 7, 1993®

ABSTRACT: In this paper we use the polymer adsorption theory of Scheutjens and Fleer to describe polymer brushes at spherical and cylindrical surfaces that are immersed in a low molecular weight solvent. We analyze the volume fraction profiles of such brushes, focusing our attention on spherical brushes in athermal solvents. These are shown to generally consist of two parts: a power law-like part and a part that is consistent with a parabolic potential energy profile of the polymer segments. Depending on the curvature of the surface, one of these two parts is more important, or may even dominate completely. We especially consider the distribution of the free end segments and the possible existence of a "dead zone" for these segments. Such a dead zone is actually found and is seen to follow a scaling law in the case of large curvatures. Furthermore, the effect of diminishing the solvent quality is considered for both the total volume fraction profile and the distribution of the end segments.

1. Introduction

Over the past years much effort has been put into the theoretical description of so-called polymer brushes: systems in which polymer chains are end-attached to an interface. Scaling analyses,[1,2] self-consistent field (SCF) theories,[3-6] and Monte Carlo[3,7-9] and molecular dynamics simulations[10] have been developed for and applied to these systems. Originally, they were used to describe polymer brushes at flat interfaces, but recently several papers have appeared whose aim it is to describe curved interfaces.[11-13] Especially in the case of an analytical SCF theory it is a challenging and certainly not a trivial step to extend models for flat systems to a curved geometry. The relevance of this extension is, however, self-evident. Polymer brushes can be seen as a model for adsorbed diblock copolymer layers which are able to stabilize colloidal dispersions. Generally, the surface of colloidal particles is not flat, but may easily have a radius of curvature that is comparable to the thickness of the adsorbed polymeric layer. A model based on polymers grafted to a convex interface can also be used to study solutions and melts of block copolymers under the conditions in which microphases are formed. Star-shaped polymers can be studied by using their similarity to linear chains that are grafted onto a small spherical particle.

The conceptually most simple model of a polymer brush is the scaling picture due to Alexander and de Gennes,[1,2] which assumes a step-like concentration profile with all chain ends situated on the outer side of the polymer layer. Using straightforward geometrical arguments, this model was later extended by Daoud and Cotton to spherical interfaces[14] and by Birshtein *et al.* to cylindrical interfaces.[15,16] For such curved interfaces, the volume fraction profile becomes dependent on the distance to the grafting surface:

$$\phi(z) = \sigma^{(3\nu-1)/2\nu}\left(\frac{R}{R+z}\right)^{(d-1)(3\nu-1)/2\nu} \qquad (1)$$

where ϕ is the volume fraction, σ is the grafting density, R is the radius of curvature of the grafting surface, z is the distance to the surface (so that $r = R + z$ is the distance to the center of the sphere or cylinder, see Figure 1), and ν is the Flory exponent, which depends upon the solvent quality ($\nu = 3/5$ for a good solvent, $\nu = 1/2$ for a Θ-solvent, and $\nu = 1/3$ for a nonsolvent). The dimensionality d is determined by the geometry of the grafting surface: d = 1, 2, and 3 for planar, cylindrical, and spherical surfaces, respectively.

A more sophisticated approach to the structure of a grafted polymer layer (at a flat surface) using self-consistent field (SCF) arguments was given in the papers of Zhulina, Borisov, and Priamitsyn[6,17] and of Milner, Witten, and Cates.[4,5] These are all based on an idea by Semenov[18] that when a polymer chain is strongly stretched with respect to its Gaussian dimensions, it is possible to replace its set of conformations by an "average trajectory", thus significantly simplifying the description of the system. This concept was first used by Semenov to study superstructure formation in block copolymer melts. Later the SCF approach was generalized and it has been applied to grafted polymer layers immersed in both low molecular weight solvents[5,17] as well as solutions and melts of mobile polymers.[19] Furthermore, nonequilibrium effects such as the deformational[4] and dynamical[20] behavior of grafted layers were studied. These investigations have led to a different overall picture of the planar grafted polymer layer structure as compared to the scaling approach. The polymer concentration decreases monotonically on going away from the grafting surface, and free chain ends are distributed throughout the whole layer. The precise form of the total concentration profile as well as that of the chain end distribution function depend on parameters such as solvent quality and polydispersity. In this pioneering publication Semenov[18] already showed that in cylindrical and spherical convex layers the free chain ends must be excluded from the vicinity of the grafting surface. Ball *et al.*[11] were the first to extend this SCF approach in a rigorous manner to chains grafted to a convex interface. They derived analytical solutions for the case of densely grafted chains at a cylindrical interface immersed in a melt. With increasing radius of curvature an exclusion zone with an increasing height appears next to the surface. Free chain ends are excluded from this zone.

For the cases of spherical interfaces and brushes with solvent, equations were given that still need to be solved (numerically). Ball *et al.* anticipate that under these conditions the distribution of free ends will remain qualitatively the same.

* To whom correspondence should be addressed.
† Permanent address: Institute of Macromolecular Compounds, Russian Academy of Science, St. Petersburg 199004, Russia.
® Abstract published in *Advance ACS Abstracts*, November 15, 1993.

0024-9297/93/2226-7214$04.00/0

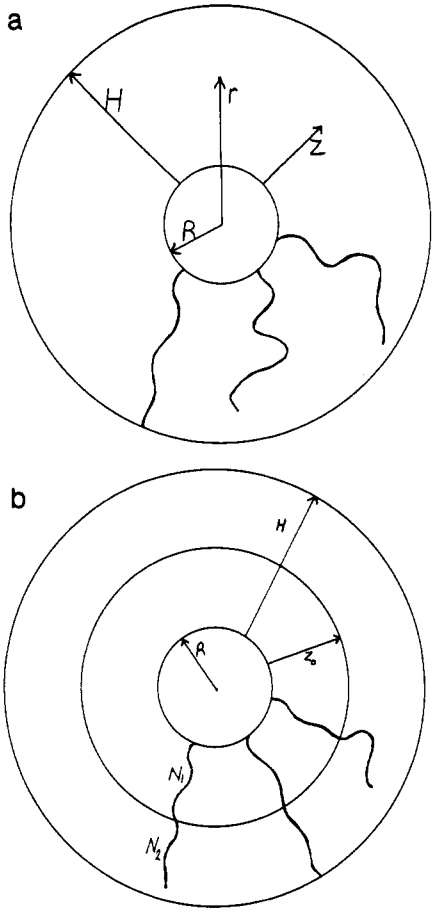

Figure 1. (a) Polymer chains that are end-attached to a curved surface with radius of curvature R form a brush of height H. The distance to the center of the sphere or cylinder is r, and z denotes the distance to the surface. (b) For intermediate values of R the polymer brush can be divided into two parts. From $z = 0$ to $z = z_0$ all chains are stretched equally. Segment N_1 of every chain is situated at a distance z_0 from the surface. The remaining $N_2 = N - N_1$ segments are subject to a parabolic potential profile in the region $z = z_0$ to $z = H$.

Simulations of star-shaped polymers using a molecular dynamics method[21] do indeed suggest that in a spherical geometry the dead zone exists for brushes in a good solvent. However, simulations of chains grafted to a cylindrical surface in a good solvent[12] do not show this dead zone, except for $R \to 0$ (i.e., the cylinder is reduced to a single line). The molecular dynamics simulations of ref 21 confirm the scaling prediction of eq 1 for $d = 3$.

Recently, Dan and Tirrell[13] have applied the Edwards diffusion equation approach[22] to end-attached polymer chains. They extended the numerical procedure by Dolan and Edwards[23] for grafted chains at a flat surface to cylindrical and spherical surfaces. Especially for cylindrical surfaces the scaling predictions agree badly with their results. Dan and Tirrell, who are investigating brushes in a good solvent, do find dead zones near the surface which agree fairly well with the predictions of Ball *et al.* for brushes in a melt.

In this paper we present results from SCF lattice calculations on end-grafted chains at cylindrical and spherical surfaces in the presence of solvents of various qualitites (very bad to very good). The model we use is an extension of the polymer adsorption theory of Scheutjens and Fleer[24,25] for curved geometries, which in its basic assumptions is very similar to the diffusion equation approach. However, within the approximation of using a mean-field lattice model, all properties of the system under consideration can be calculated exactly. No further approximations are needed. For example, we need not assume that the polymer segment potential is proportional to the local segment density (as must be done in the numerical procedure of ref 23). Also any solvent quality can be chosen. In the next section we will go into further details concerning the lattice model. In section 5 we will show results of this model and (where possible) compare them with predictions from one of the models mentioned above. First we shall, however, introduce two analytical models in sections 3 and 4 to describe brushes in good and Θ-solvents at curved surfaces. In section 5 we will also see under what conditions these models are valid by comparing them with the lattice model calculations. In doing so, we will focus our attention on spherical brushes in athermal solvents.

2. Self-Consistent Field Lattice Model

In the polymer adsorption theory of Scheutjens and Fleer[24,25] the equilibrium distribution of a polymer–solvent system at an interface is calculated by taking into account all possible conformations, each weighted by its Boltzmann probability factor. Cosgrove *et al.*[3] and Hirz[26] showed that this method can be applied to terminally attached chains by restricting the allowed conformations to those whose first segment is in the layer adjacent to the surface. In a previous paper[27] we described this modified procedure and used it to calculate characteristics of polymer brushes on flat surfaces. The basic principles of the model can also be applied in a lattice with a curved geometry, as was first demonstrated by Leermakers and Scheutjens,[28] who used such a lattice to study lipid vesicles and surfactant micelles. In this section we shall briefly review the relevant geometrical aspects of their approach.

The differences between a curved and a planar lattice are that the number of sites in a layer increases on moving away from the center of the lattice and that the lattice transition parameters λ_-, λ_0, and λ_+ are layer dependent. A lattice site in layer r has neighboring sites in layers $r - 1$, r, and $r + 1$. A fraction λ_- of these neighboring sites are in layer $r - 1$, a fraction λ_0 are in layer r, and a fraction λ_+ are in layer $r + 1$. We number the layers $r = 1, 2, 3,...$ starting from the center of the sphere or cylinder. Applying the condition that all layers are equidistant, one finds that the volume $V(r)$, expressed in number of lattice sites, enclosed by layer r equals:

$$V_d(r) = \frac{C_d}{d}(r)^d \tag{2}$$

where $d = 3$ for a spherical and $d = 2$ for a cylindrical lattice (and $d = 1$ for a flat lattice). This volume is defined per surface area for $d = 1$, per length unit for $d = 2$, and per sphere for $d = 3$. The numerical constant C_d has the values $C_1 = 1$, $C_2 = 2\pi$, and $C_3 = 4\pi$. The number of lattice sites in layer r is given by $L(r) = V(r) - V(r - 1)$, or

$$L_d(r) = \frac{C_d}{d}((r)^d - (r-1)^d) \tag{3}$$

Differentiating $V(r)$ with respect to r gives the surface area $S(r)$ of layer r:

$$S_d(r) = C_d(r)^{d-1} \tag{4}$$

The transition factors $\lambda_-(r)$ and $\lambda_+(r)$ are proportional to the surface area per site in contact with the adjacent layer, so that,

$$\lambda_{+d}(r) = \lambda_{+1}\frac{S_d(r)}{L_d(r)}$$

$$\lambda_{-d}(r) = \lambda_{-1}\frac{S_d(r-1)}{L_d(r)}$$

$$\lambda_{0d}(r) = 1 - \lambda_{+d}(r) - \lambda_{-d}(r) \quad (5)$$

where λ_{+1} and λ_{-1} are the values of the transition factors for the equivalent planar lattice. In all calculations presented in this paper we have used a cubic lattice, for which $\lambda_{+1} = \lambda_{-1} = {}^1/_6$. In a flat geometry ($d = 1$) the cubic lattice gives an equal a priori probability to a bond between two segments in any of the four directions parallel to the surface as well as to a bond toward the surface or away from the surface. This is in accordance with the underlying physical model of refs 4 and 6. We emphasize an important consequence of our definition of the transition probabilities. It follows from eqs 3 and 5 that

$$\lambda_{-d}(r)L_d(r) = \lambda_{+d}(r-1)L_d(r-1) \quad (6)$$

which means that the condition is satisfied that the statistical weight of a polymer conformation does not depend upon the chain end at which we start to evaluate this quantity.

When studying polymer grafted at a solid–liquid interface with a radius of curvature R, we must exclude the layers $r = 1, 2, 3,\ldots R$ from our system. We number our layers $z = 1, 2, 3,\ldots$ starting from layer $r = R + 1$ ($z = 1$), which is adjacent to the solid–liquid interface (see also Figure 1). The actual calculation of the equilibrium distribution of a polymer–solvent system now takes places completely analogously to the procedure described in ref 27. Only the transition parameters of eq 2 of this reference must be replaced by the appropriate expressions from our eq 5, and the denominator of eq 6 in ref 27 becomes $\sum_z L(z)G(z,N)$. Of course the procedure described above can not only be used to compute systems with end-grafted polymer but also for polymer adsorption from solution. In a future publication we intend to present results thus found for homo- and block copolymer adsorption on spherical colloidal particles.

As described in ref 27 a numerical iteration scheme is applied to find the self-consistent volume fraction profile of the polymer. Due to mathematical complexity, the equations cannot be solved exactly using analytical methods. In the next section we will discuss less-exact SCF approaches to our system of curved brushes, which enable us to find analytical approximations for the volume fraction profile.

3. Analytical SCF Model

Large Curvature. We will start by considering polymer chains that are end-attached to a spherical interface with a small radius of curvature (i.e. brushes with a large curvature). We make the simplifying approximation that the free ends of all chains are situated at the same distance H from the surface. The elastic chain-stretching contribution to the free energy of the system for an arbitrary geometry (planar, cylindrical, or spherical) can then be written as

$$A_{el} = \frac{3f_d}{2a^2}\int_0^H\left(\frac{dz}{ds}\right)dz = \frac{3af_d^2}{C_d}\int_0^H\frac{dz}{(z+R)^{d-1}\phi(z)} \quad (7)$$

and is defined per surface area in the planar case ($d = 1$), per length unit in the cylindrical case ($d = 2$), and per sphere for the spherical geometry ($d = 3$). The local chain stretching at distance z from the surface is given by ds/dz, and $f_d = \sigma S_d(R)$ is the number of chains. In distinction to the previous section the distance z to the surface is now a continuous variable. Because of the equal stretching of all chains

$$\phi(z) = \frac{f_d a^3 ds}{S_d(z+R)}dz$$

The contribution to the free energy of the system due to the mixing of grafted chains and solvent molecules can be written as a virial expansion,

$$A_{mix} = \int_0^H dz\,(v\phi^2(z) + w\phi^3(z))S_d(z+R) \quad (8)$$

where v and w are the second and third virial coefficients (within Flory theory $v = 0.5 - \chi$ and $w = {}^1/_6$). The free energy functional $A_{el} + A_{mix}$ must be minimized under the constraint

$$\frac{1}{f_d a^3}\int_0^H dz\,\phi(z)S_d(z+R) = N \quad (9)$$

For a given height H this leads to the equation

$$\frac{R^{d-2}\sigma^2}{(z+R)^{2d-2}\phi^2(z)} = \frac{4}{3}v\phi(z) + 2w\phi^2(z) + \Lambda \quad (10)$$

where Λ is an undetermined Lagrangian multiplier. Solving $\phi(z)$ from this equation and substituting it into eq 9 one can find Λ. Minimization of the total free energy $A_{el} + A_{mix}$ with respect to H gives the volume fraction profile for given values of R and σ. Under good solvent conditions and for large curvatures, the two last terms in eq 10 may be neglected, so that[29]

$$\phi(z) = \left(\frac{3\sigma^2}{4v}\right)^{1/3}\left(\frac{R}{z+R}\right)^{(2d-2)/3} \quad (11)$$

Substituting this expression into eq 9 we find the following scaling law for the layer height:

$$H \sim (N^3R^{d-1}\sigma v)^{1/(d+2)} \quad (12)$$

In a Θ-solvent ($v = 0$), omitting the first and last terms on the right hand side of eq 10 leads to

$$\phi(z) = \left(\frac{\sigma^2}{2w}\right)^{1/4}\left(\frac{R}{z+R}\right)^{(2d-2)/4} \quad (13)$$

We conclude that in a spherical convex brush $\phi(z)$ scales as $(z+R)^{-4/3}$ in a good solvent, and $\phi(z) \sim (z+R)^{-1}$ in a Θ-solvent. In a cylindrical brush $\phi(z) \sim (z+R)^{-2/3}$ in a good solvent, and $\phi(z) \sim (z+R)^{-1/2}$ in a Θ-solvent. This is in agreement with eq 1. In bad solvents $\phi(z) \sim z^0$ for all three geometries. In a bad solvent ($v < 0$) the left-hand side of eq 10 can be neglected, so that

$$\phi(z) = \frac{|v|}{3w} + \sqrt{\frac{v^2}{9w^2} - \frac{\Lambda}{2w}} = \text{const} \quad (14)$$

The value $\Lambda = v^2/6w$ obtained from the minimization of A_{mix} with respect to H under constraint 9 gives a well-known result for a collapsed globule.

$$\phi(z) = \frac{|v|}{2w} \quad (15)$$

Small Curvature. We will now discuss the opposite case of small curvature (R is large). We limit ourselves to good solvents and spherical surfaces. Other geometries and solvent qualities can be described along similar lines. Of course, for infinitely large radii of curvature the polymer

brush is described by a parabolic potential profile, which in a good solvent leads to a brush height H_0 given by the equation,

$$H_0 = \left(\frac{8}{\pi^2}\right)^{1/3} aNv^{1/3}(a^2\sigma)^{1/3} \tag{16}$$

where N is the degree of polymerization, a the segment diameter, v the second virial coefficient, and σ the grafting density. Following Liatskaya *et al.*[30] and Milner *et al.*,[31] we assume that for low curvatures it is still a good approximation to describe the polymer brush by a parabolic potential profile. The brush height H will then depend upon the relative curvature, ω^{-1}, which we define as the ratio of the flat brush height and the radius of curvature of the surface, $\omega = R/H_0$. In a good solvent this height H at a spherical surface is given by the equation

$$\left(\frac{H}{H_0}\right)^3\left(1 + \frac{3H}{4\omega H_0} + \frac{1}{5}\left(\frac{H}{\omega H_0}\right)^2\right) = 1 \tag{17}$$

The corresponding volume fraction profile is

$$\phi(z) = \frac{3\sigma N a^3}{H_0}\left(\frac{H}{H_0}\right)^2\left(1 - \left(\frac{z}{H}\right)^2\right) \tag{18}$$

and the distribution function of free ends:

$$g(z) = \frac{3zH^2}{H_0^3}\left\{\left[2 + \frac{3H}{\omega H_0} - \frac{2}{3}\left(\frac{H}{\omega H_0}\right)^2 + \frac{8}{3}\left(\frac{H}{\omega H_0}\right)^2\left(\frac{z}{H}\right)^2\right]\sqrt{1 - \left(\frac{z}{H}\right)^2} - \frac{H}{\omega H_0}\left(2 - 3\left(\frac{z}{H}\right)^2\right)\ln\left(\frac{1 + \sqrt{1 - \left(\frac{z}{H}\right)^2}}{\frac{z}{H}}\right)\right\} \tag{19}$$

This result was previously derived by Liatskaya *et al.*[30] The approximations made in this model turn up when one examines the function $g(z)$. For low values of z it becomes negative. Of course a probability smaller than zero has no physical meaning. It is possible to interpret the zone where $g(z) \leq 0$ as an area where no end segments are located. We define Δ_p as the size of this "dead zone", so that $g(\Delta_p) = 0$. The value of Δ_p (where the subscript p stands for parabolic) depends on the curvature of the surface. Figure 2a shows the relative thickness of the dead zone, Δ_p/H, as a function of R/H. The maximum relative value for the dead zone is reached in the limit $R/H \to 0$, when $\Delta_p = H/2$. When $R/H \ll 1$ the layer height scales as $R^{2/5}N^{3/5}\sigma^{1/5}$, so that the absolute value of the dead zone ($\Delta_p \sim H \sim R^{2/5}$) increases with R and passes through a maximum at $R/H \approx 1$, as can be seen in Figure 2b. For small curvatures ($R/H \gg 1$) Δ_p decays exponentially with R.

Intermediate Curvatures. For intermediate radii of curvature we make the approximation that the volume fraction profile is a combination of the two previously discussed profiles. Up to a distance z_0 from the surface (see Figure 1b) all chains are stretched equally. Per chain there are N_1 segments in this part of the brush. The other N_2 segments are situated in a parabolic potential profile and can be thought of as being grafted to an imaginary radial surface with radius $R + z_0$. For a spherical layer in a good solvent this leads to the following overall profile:

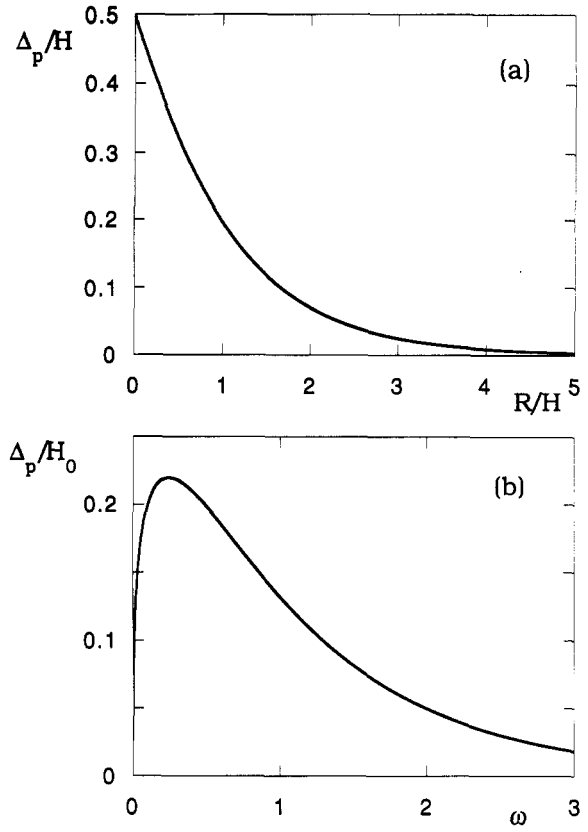

Figure 2. (a) The behavior of the dead zone for free ends in the parabolic potential approximation. Δ/H is given as a function of R/H (Δ: dead zone size, H: layer height, R: radius). Note that H itself depends on R for a given chain length. (b) The ratio of dead zone length, Δ, and flat brush height, H_0, is given as a function of the relative radius of curvature, ω.

$$\phi(z) = \begin{cases} \left(\frac{3}{64\pi^2}\right)^{1/3}\frac{f^{2/3}v^{-1/3}a^{4/3}}{(R+z)^{4/3}} & \text{for } 0 \leq z \leq z_0 \\ \frac{3\pi^2}{16a^2N_2^2v}(H^2 - (z - z_0)^2) & \text{for } z_0 \leq z \leq H + z_0 \end{cases} \tag{20}$$

where $f = f_3$ is the number of chains per sphere ($f = 4\sigma\pi R^2$). The values of N_1, N_2, H, and z_0 follow from the three conditions:

(1) continuity of the profile at $z = z_0$:

$$\left(\frac{3}{64\pi^2}\right)^{1/3}\frac{f^{2/3}v^{-1/3}a^{4/3}}{(R+z)^{4/3}} = \frac{3\pi^2}{16a^2N_2^2v}H^2 \Rightarrow$$

$$H = \frac{2a^{5/3}N_2v^{1/3}f^{1/3}}{3^{1/3}\pi^{4/3}(R+z_0)^{2/3}} \tag{21}$$

(2) conservation of segments in the inner layer:

$$fN_1a^3 = \int_0^{z_0}\phi_1 4\pi(R+z)^2dz \Rightarrow$$

$$N_1 = \frac{3(3\pi)^{1/3}v^{-1/3}f^{-1/3}}{5a^{5/3}}((R+z_0)^{5/3} - R^{5/3}) \tag{22}$$

(3) conservation of segments in the outer layer:

$$fN_2a^3 = \int_{z_0}^{z_0+H}\phi(z)4\pi(R+z)^2dz \Rightarrow$$

$$\frac{\pi^3(R+z_0)^2H^3}{2a^5N_2^3vf}\left(1 + \frac{3H}{4(R+z_0)} + \frac{H^2}{5(R+z_0)^2}\right) = 1 \tag{23}$$

Rearranging these equations and introducing $u = z_0/R$,

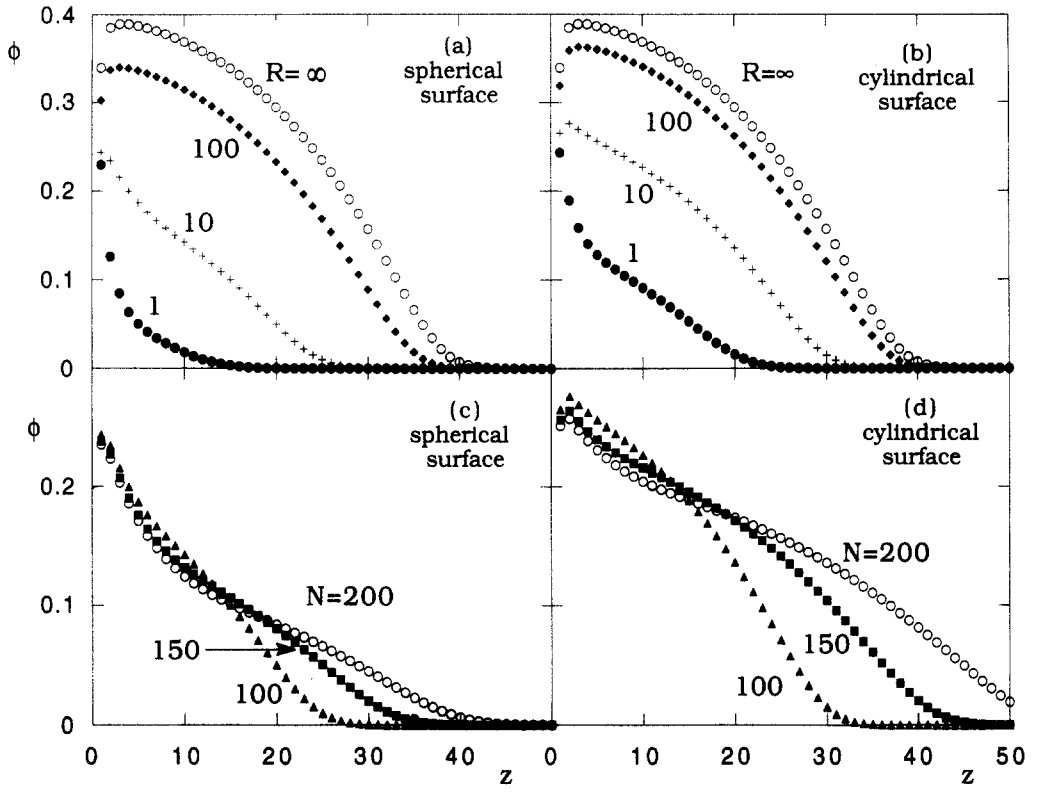

Figure 3. Effect of radius of curvature and chain length on the segment distribution in spherical and cylindrical geometries. (a and b) Chain length $N = 100$; (●) $R = 1$, (+) $R = 10$, (◆) $R = 100$, (○) $R = \infty$. (c and d) $R = 10$; (▲) $N = 100$, (■) $N = 150$, (○) $N = 200$. (a and c) Spherical geometry; (b and d) cylindrical geometry. In all cases $\chi = -0.5$.

one can write,

$$u = \left(\frac{1 + \frac{5}{3}\left(\frac{\pi^2}{6}\right)^{1/3} \omega^{-1}}{1 + \frac{5}{6}\pi c} \right)^{3/5} - 1 \qquad (24)$$

where the constant c is defined by

$$c = -\frac{15}{8} + \sqrt{\frac{225}{64} + 5\left(\frac{3\pi}{4} - 1\right)} \approx 1.334 \qquad (25)$$

We now define a critical relative curvature, ω_{cr}, so that for $\omega > \omega_{cr}$ the potential profile is parabolic, whereas for $\omega < \omega_{cr}$ the volume fraction profile is a combination of both models. For $\omega < \omega_{cr}$ there is a zone $\Delta = z_0 + \Delta_p$ where no end segments are located. For a spherical brush $\omega_{cr} \approx 0.563$.

For a cylindrical layer in a good solvent the similar procedure gives $\omega_{cr} = (4/3\pi)^{1/3}(2\pi - 8/3)^{-1} \approx 0.207$. For a cylindrical brush a parabolic potential profile may be assumed over a wider range of curvatures than for a spherical brush. The combined profiles for Θ- and bad solvents in spherical and cylindrical geometries can be found in the same manner.

4. Results

The effects of surface curvature and chain length on the volume fraction profiles of brushes at spherical and cylindrical surfaces is shown in Figure 3. Here a very good solvent has been used ($\chi = -0.5$), which gives slightly more extended brushes than an athermal solvent. Parts a and b are drawn for a (relatively) short chain length of 100 segments. For low curvatures the profile has a large resemblance with the profile of a brush on a flat surface ($R = \infty$), which is also drawn for comparison. Upon increasing the curvature, the shape of a growing part of the profile becomes convex. The same trend can be seen in parts c and d, where curves are drawn for different chain lengths but with the same radius of curvature. Increasing the chain length has a similar effect on the shape of the profiles as decreasing the radius of curvature. The parameters in Figure 3 are the same as those in Figures 2 and 3 of Dan and Tirrell's paper,[13] which were calculated with an excluded volume parameter $v = 1$. The shape of our profiles is very similar to theirs. However, Dan and Tirrell consistently predict layers that are slightly more strongly stretched and consequently slightly less dense. For example, for a spherical interface with $R = 100$ and $N = 100$, they calculate a brush height that is approximately 10% larger than ours. Probably this is due to the way solvent–segment interactions are taken account of by the excluded volume parameter. As stated above, all our calculations were done using a cubic lattice. For a flat interface this lattice gives exact correspondence with the SCF theory of Zhulina *et al.* and Milner *et al.* in the limit of infinite chain length.[27]

Figure 4 gives the brush thickness as a function of polymer chain length under various conditions. This thickness has been calculated in two different ways. First, we have defined an average brush height H_{av} in a similar fashion as in ref 13,

$$H_{av} = \left(\frac{\sum_z z^2 (z + R)^2 \phi(z)}{\sum_z (z + R)^2 \phi(z)} \right)^{1/2} \qquad (26)$$

which is basically a second moment of the volume fraction profile. Secondly, we have calculated the hydrodynamic layer thickness, H_{hy}, using the theory of Cohen Stuart *et al.*,[32] taking the hydrodynamic constant $C_H = 1$. To apply this theory to curved surfaces we assume that all solvent flow takes place concentrically with respect to the surface (the flow has no component in a direction perpendicular to the surface). For low Reynolds numbers this seems a reasonable approximation for many practical systems.

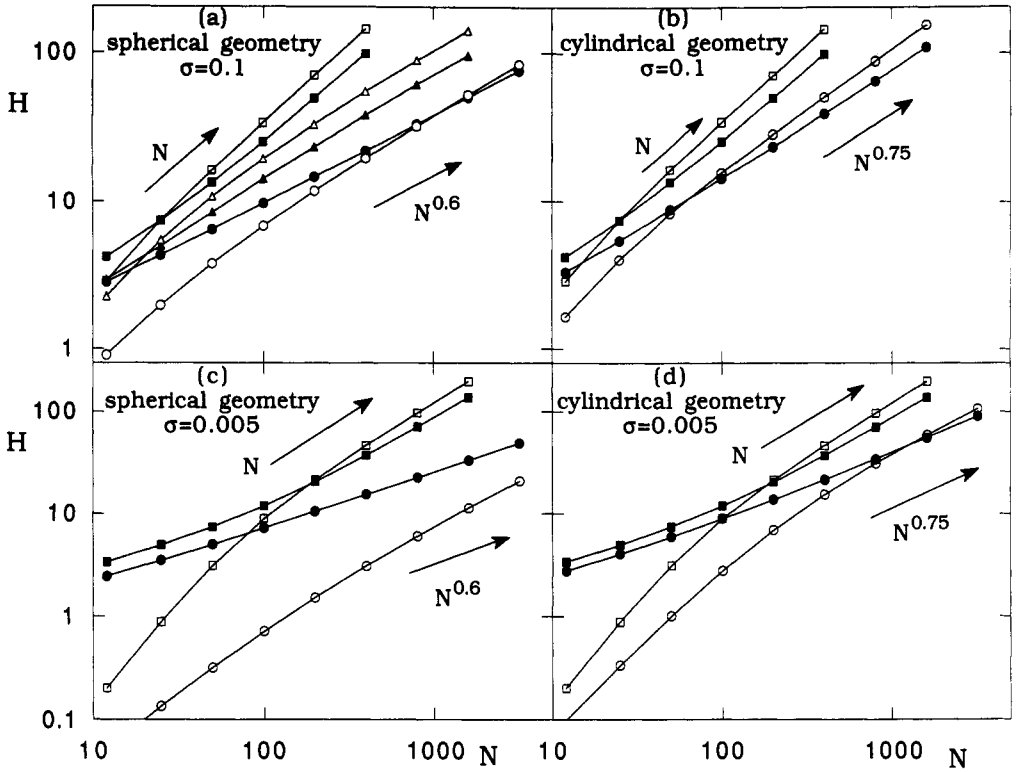

Figure 4. Brush thickness as a function of chain length in an athermal solvent. The brush thickness has both been expressed as the average segment height and as the hydrodynamic thickness (see text). Parameters: (a and c) spherical geometry; (b and d) cylindrical geometry; (a and b) $\sigma = 0.1$; (c and d) $\sigma = 0.005$. Symbols: (●) $R = 1$; (▲) $R = 10$; (■) $R = \infty$. Open symbols are hydrodynamic heights; filled-in symbols are average heights.

(Both H_{av} and H_{hy} give smaller values than the brush height H as defined in for example ref 17.) When the grafting density is high ($\sigma = 0.1$) we find very good agreement with the scaling law $H_{av} \sim N$ for a flat surface, and for a spherical surface with $R = 1$ (star-shaped polymer) we find equally good agreement with the scaling law $H_{av} \sim N^{0.6}$. For cylindrical surfaces the expected scaling behavior $H_{av} \sim N^{0.75}$ is found for $R = 1$. When $\sigma = 0.005$ increasing deviations occur from these power laws, which for flat surfaces are caused by the "foot of the parabolic profile".[27,33] The hydrodynamic thicknesses agree less well with the predicted power law. Experimentally the hydrodynamic thickness may, however, be the most easily accessible parameter for defining brush thicknesses in these systems.

In Figure 5 lattice volume fraction profiles (full curves) are given for $N = 500$ in a spherical geometry with $\sigma = 0.1$ and $\sigma = 0.005$ ($\sigma = 0.1$ is a very high grafting density, which won't easily be reached by adsorbing block copolymers, but which may be a good value for modeling a star polymer (when $R = 1$); $\sigma = 0.005$ is a more reasonable value for the grafting density on sterically stabilized colloidal particles). The dashed curves have been calculated with the equations of section 3. The curves for $R = 500$ and $R = 100$ (when $\omega > \omega_{cr}$) are given by the parabolic potential profile approximation. For smaller values of R (when $\omega < \omega_{cr}$) the "combined model" gives a reasonably good fit with the lattice calculations. The dashed curves for $\sigma = 0.005$ and $R = 5$, and $R = 1$ follow directly from eq 11. For these small values of R the "fixed chain ends" model agrees best with the lattice calculations.

Figure 6 shows how the solvent quality influences the polymer brushes. As is the case with flat brushes, a worse solvent gives a more compact grafted layer. For $\chi \approx 1$ the volume fraction profile is well approximated by a step profile, irrespective of the interface curvature, in agreement with eq 14 (of course, the height of the brush does depend on the curvature). When the curvature is not too large ($R = 100$ in Figure 6a) a brush can still be reasonably well described by the parabolic potential profile approximation applied in a Θ-solvent. For $R = 1$ the exponent of the initial decay of the profile gradually changes from $^4/_3$ to 1 when the solvency changes from $\chi = 0$ to $\chi = 0.5$.

Figure 7 gives the exact distribution functions of free chain ends of the polymer chains. The function $g(z/H_{av})$ is drawn, where H_{av} is given by eq 26 and $g(z) = \phi(z,N)L_d(z)/\sigma L_d(1)$ with $\phi(z,N)$ the volume fraction profile of the end segments. Figure 7 illustrates the existence of a dead zone in both the spherical and cylindrical geometries. Of course the probability that an end segment is located in this zone is not absolutely zero, but very small. As long as $\sigma < 1$, a polymer chain conformation with an end segment bending back to the surface will have a finite probability. This makes it difficult to speak about the absolute size of the dead zone within our lattice SCF model. One can only use an arbitrary definition for the dead zone, for example the area where $g(z)$ is smaller than 5% of its maximum value.[13] Some conclusions concerning the behavior of this zone can be drawn from Figure 7. When the radius of curvature is small, an increase in R leads to a larger dead zone, both in absolute terms (which is partly caused by an increase in the layer height) and in relative terms (as a fraction of the layer height, which can, for example, be expressed by H_{av}). Increasing R even farther at a certain point leads to a decrease of the dead zone size and eventually results in its total disappearance. These trends are clearly seen in parts a and c of Figure 7 where the grafting density is high ($\sigma = 0.1$). For the far lower grafting density of 0.005, which in many practical systems may still be a very realistic value, the dead zone is significantly smaller.

The behavior of the dead zone size as a function of surface curvature is at least qualitatively in agreement with eq 19 (parabolic potential profile) and with the combined model. In Figure 8 the chain end distribution

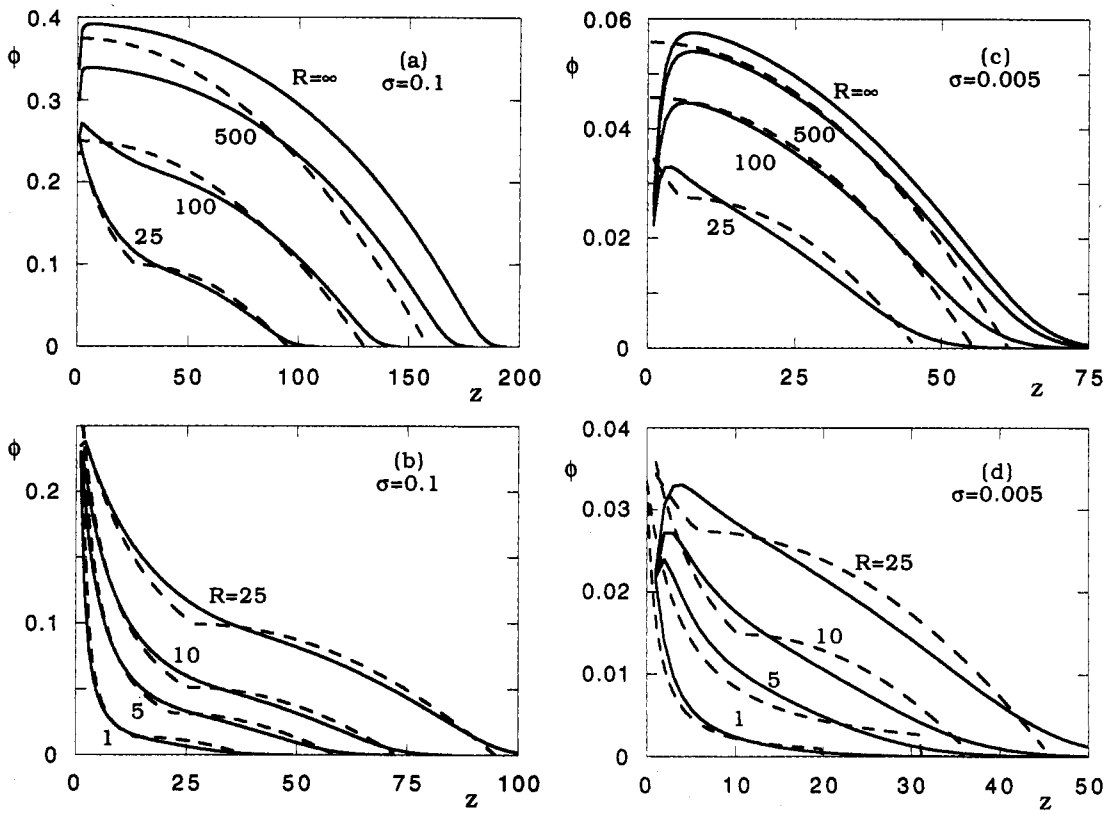

Figure 5. Volume fraction profiles for a spherical surface; $N = 500$; (a) $\sigma = 0.1$, $R = \infty$, $R = 500$, $R = 100$, and $R = 25$; (b) $\sigma = 0.1$, $R = 25$, $R = 10$, $R = 5$, and $R = 1$; (c) $\sigma = 0.005$, $R = \infty$, $R = 500$, $R = 100$, and $R = 25$; (d) $\sigma = 0.005$, $R = 25$, $R = 10$, $R = 5$, and $R = 1$. In all cases $\chi = 0$. The full curves are lattice calculations. For $R = 500$ and $R = 100$, the dashed curves are the "parabolic potential profile" approximation. In d the dashed curves for $R = 1$ and $R = 5$ follow from the "fixed chain ends" model. All other dashed curves were calculated according to the combined model.

g is given as a function of z as calculated from the lattice model (full curves), and the parabolic potential model and the combined model (dashed curves) for grafting densities of 0.1 and 0.005. There is a fair correspondence between the lattice calculations and the predictions of section 3. In the parabolic potential model the negative values of g for small z must be compensated by too large values of g elsewhere. This is the main reason for the differences found around the maximum of $g(z)$. Nevertheless, for all sets of parameters the analytical equations correctly predict the location of this maximum. The lattice calculations do consistently show a smaller dead zone and an appreciably wider distribution of free end segments at the tip of the brush. These segments are located in the "foot" of the parabolic profile. Especially for smaller values of R the differences between the two curves become significant. For very small R the end segments certainly do not all tend to be concentrated in a narrow zone (although the overall volume fraction profile, as seen above, does tend to the $-4/3$ power law of the "fixed chain end" model). Overall, the approximate analytical equations give a reasonable prediction of the dead zone size.

Figure 9 explores a possible scaling behavior of the free end distribution. Both in the limit of small particle radius and for brushes under parabolic potential conditions the brush height scales as

$$H \sim (\sigma N^3 R^{d-1})^{1/(d+2)}$$

This suggests that the free end segments and the dead zone size may have a similar scaling dependence. Figures 9a–c show the end segment distribution function g in a spherical geometry as a function of $z/(N^{3/5}R^{2/5}\sigma^{1/5})$. If the scaling law $\Delta \sim N^{3/5}R^{2/5}\sigma^{1/5}$ were correct, all curves should become 0 at the same value of $z/(N^{3/5}R^{2/5}\sigma^{1/5})$. This is not the case. A better approximation would be to assume that the dead zone is equal to the first part z_0 of the combined model. From eqs 21–23 one can then derive that

$$\frac{\Delta}{(\sigma N^3 R^{d-1})^{1/(d+2)}} = \upsilon^{1/(d+2)}\left(\frac{\left(\frac{8}{\pi^2}\right)^{1/3}\omega + \frac{d+2}{3}\left(\frac{4}{3}\right)^{1/3}}{1+\frac{d+2}{6}\pi c}\right)^{3/(d+2)} - \upsilon^{1/(d+2)}\left(\left(\frac{8}{\pi^2}\right)^{1/3}\omega\right)^{3/(d+2)}$$

$$\approx 0.509 \text{ for } \omega \to 0 \quad \text{if } d = 3$$

$$\approx 0.224 \text{ for } \omega \to 0 \quad \text{if } d = 2 \qquad (27)$$

where the constant c is given by eq 25. In the legends of Figure 9 the values of $\Delta/(N^3R^{d-1}\sigma)^{1/(d+2)}$ are also given as calculated from this equation. For short chain lengths (e.g., $R = 5$, $N = 200$, $\sigma = 0.1$; see Figure 9c) and for very low grafting densities (e.g., $R = 5$, $N = 1000$, $\sigma = 0.005$; see Figure 9b) deviations start to occur from eq 27 which are caused by the fact that the chains are not strongly stretched for these parameters. We do indeed see that for small values of ω (e.g. for $R = 5$, $N = 1000$, and $\sigma = 0.1$ we have $\omega = 0.015$) the dead zone size approaches the value given by eq 27 for $\omega \to 0$. Of course one must realize that the exact lattice calculations also take "fluctuations" into account which allow a finite number of conformations to have their end-segments bend back to the power-law part of the volume fraction profile. This is analogous to the

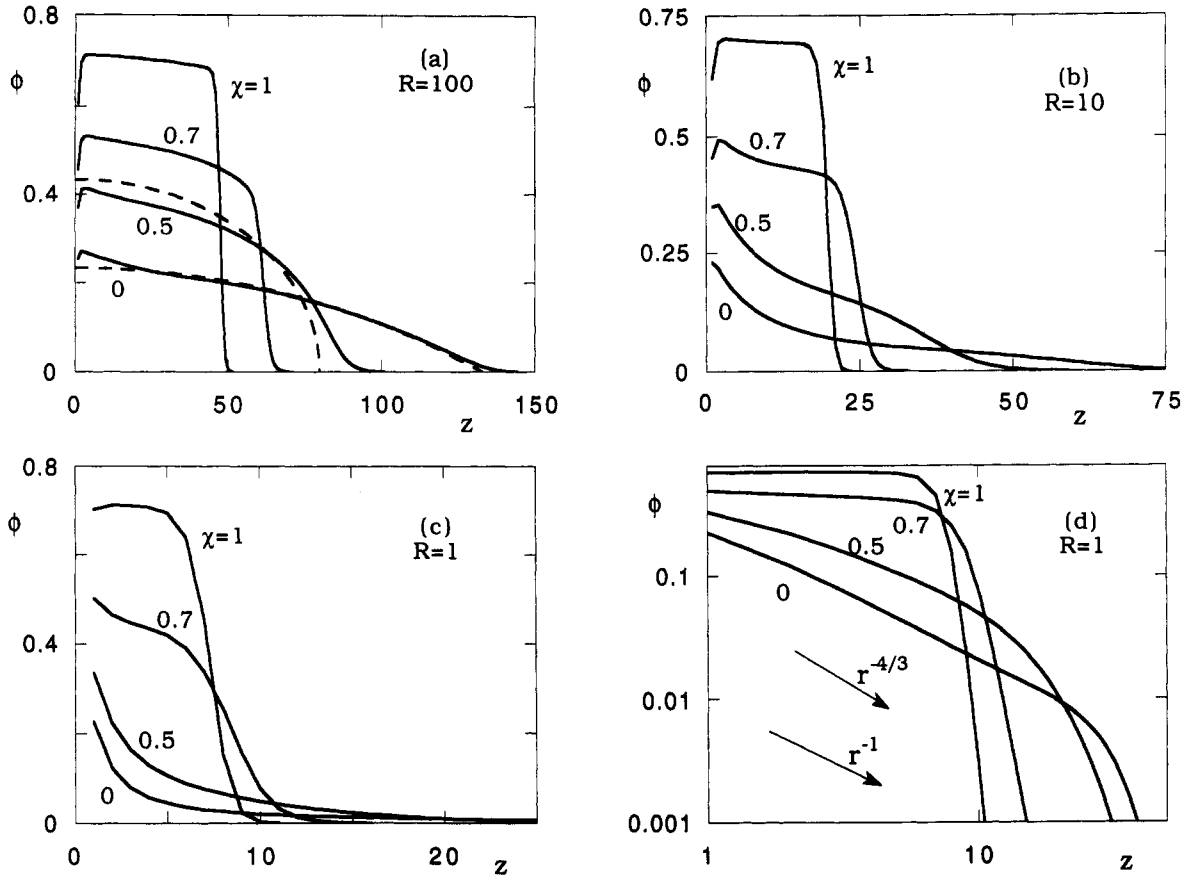

Figure 6. Volume fraction profiles in a spherical geometry for different solvent strengths: a decrease of the solvent quality leads to a collapse of the grafted layer. In a the dashed curves are the parabolic potential model predictions. For $R = 1$ the profiles are also given on a logarithmic scale to be able to check for a power law dependency between ϕ and z. Parameters: $\sigma = 0.1$; $N = 500$; $\chi = 0, 0.5, 0.7, 1$; (a) $R = 100$; (b) $R = 10$; (c and d) $R = 1$.

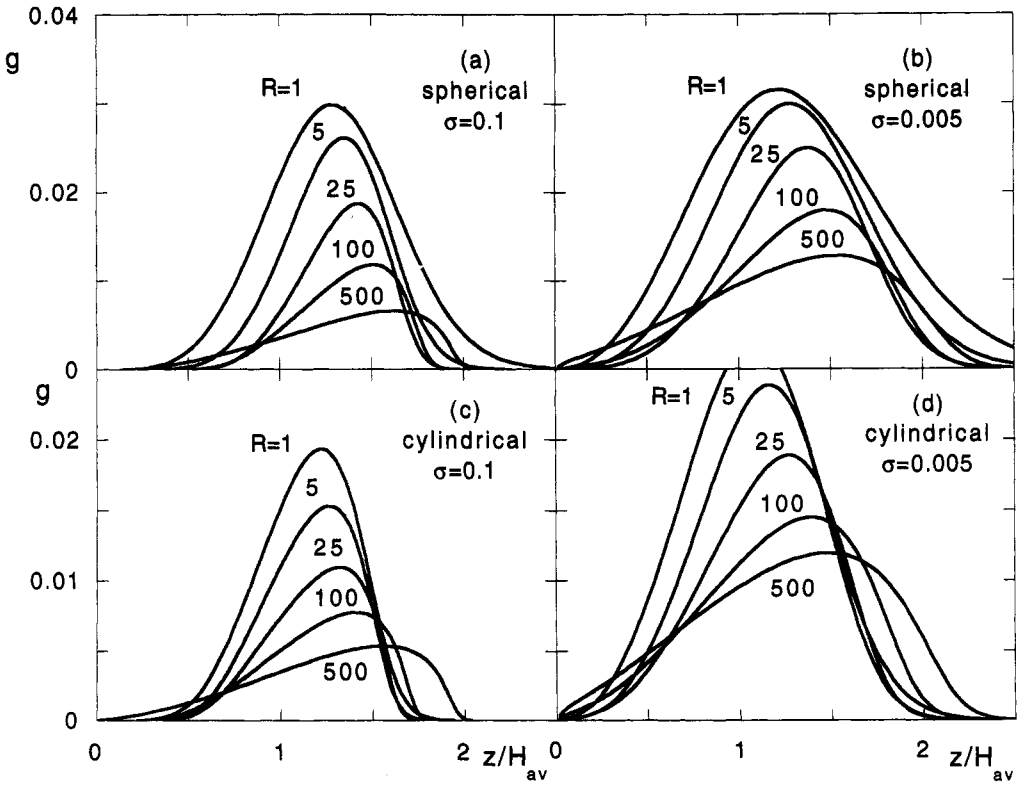

Figure 7. Free chain end distribution functions, g, as a function of the reduced distance to the surface, z/H_{av}, for various radii of curvature as indicated; (a and b) spherical geometry; (c and d) cylindrical geometry; (a and c) $\sigma = 0.1$; (b and d) $\sigma = 0.005$. Further parameters: $N = 1000$; $\chi = 0$.

"foot" that occurs in the volume fraction profile at the tip of the brush and explains why the curves do not show a sharply defined border of the dead zone. On the other hand eq 27 of course neglects the existence of a dead zone Δ_p in the parabolic potential part of the profile. For ($R = 100, N = 1000, \sigma = 0.1$; Figure 9a) one sees that the dead

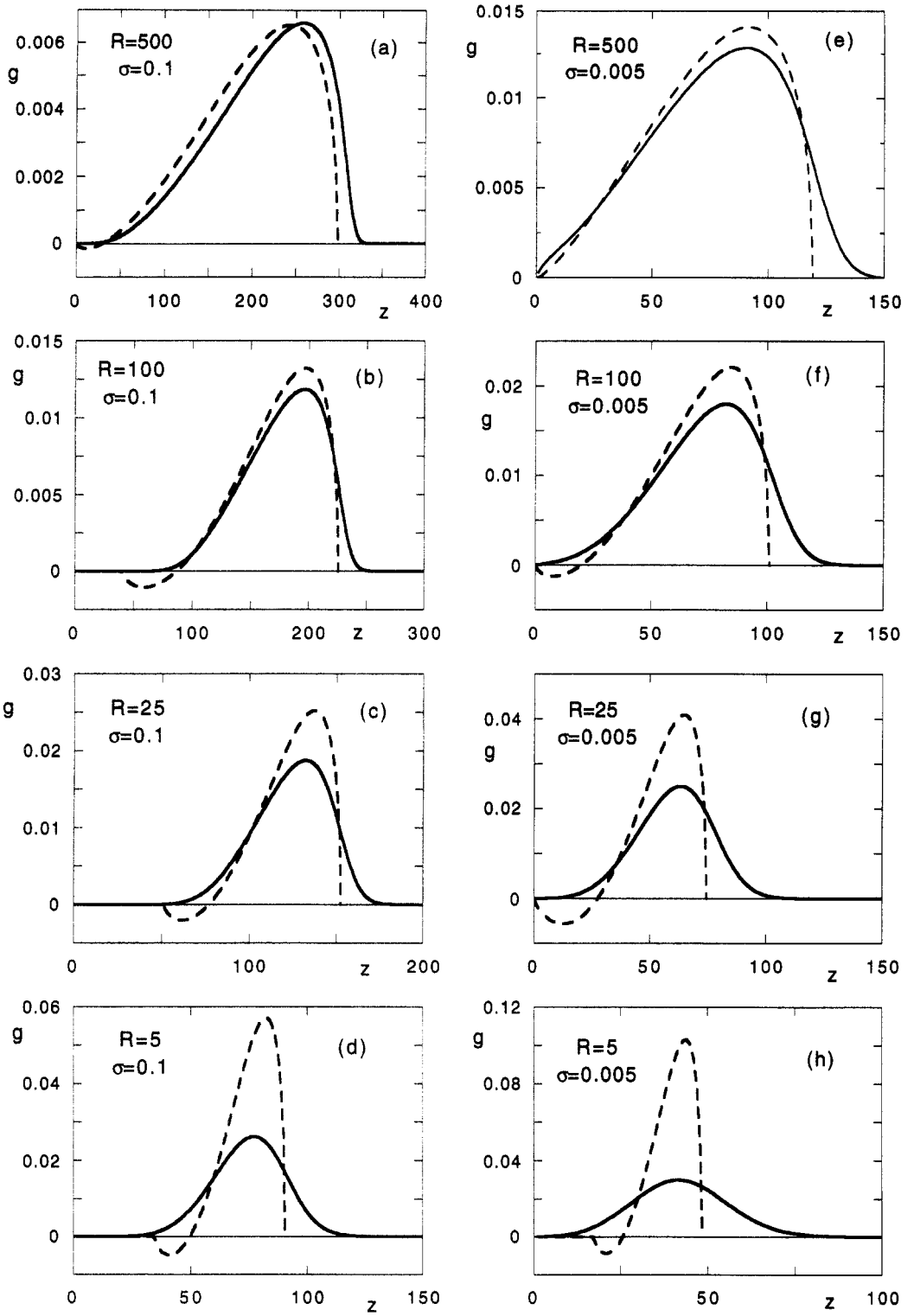

Figure 8. Free chain end distribution functions, g, as a function of z in a spherical geometry for $\sigma = 0.1$ (a–d) and $\sigma = 0.005$ (e–h). The full curves are lattice calculations, the dashed curves are the analytical equations (the parabolic potential profile model was used for a, e, f, and g, and the combined model was used for b, c, d, and h). Further parameters: $N = 1000$; $\chi = 0$.

zone is significantly larger than the value predicted by eq 27. In this case the contribution of Δ_p to the total dead zone Δ becomes apparent. Figure 9 also shows that when N and σ are changed the location of the maximum of the function $g(z/(\sigma N^3 R^{d-1})^{1/(d+2)}$ hardly changes. The area under the curves does change but this is because we have defined $\int g(z)dz = 1$. If the curves in Figures 9b and 9c are normalized so that

$$\int g(z/(\sigma N^3 R^{d-1})^{1/(d+2)}\, d(z/(\sigma N^3 R^{d-1})^{1/(d+2)}) = 1$$

all curves virtually collapse onto a master curve. This is, however, not the case for the curves in Figure 9a. Increasing the particle radius shifts the maximum in g to lower values of $z/(\sigma N^3 R^{d-1})^{1/(d+2)}$.

Figures 9d,e show the same curves as 9a–c for a cylindrical surface. Most dead zones are slightly larger than predicted by eq 27. This is caused by the contribution of Δ_p to the total dead zone Δ. The general shape of the curves shows the same behavior as in the spherical geometry. The values of Δ are smaller than those for the spherical surfaces, but the dependence of Δ upon N, R, and σ is very similar to that found in parts a–c of Figure 9.

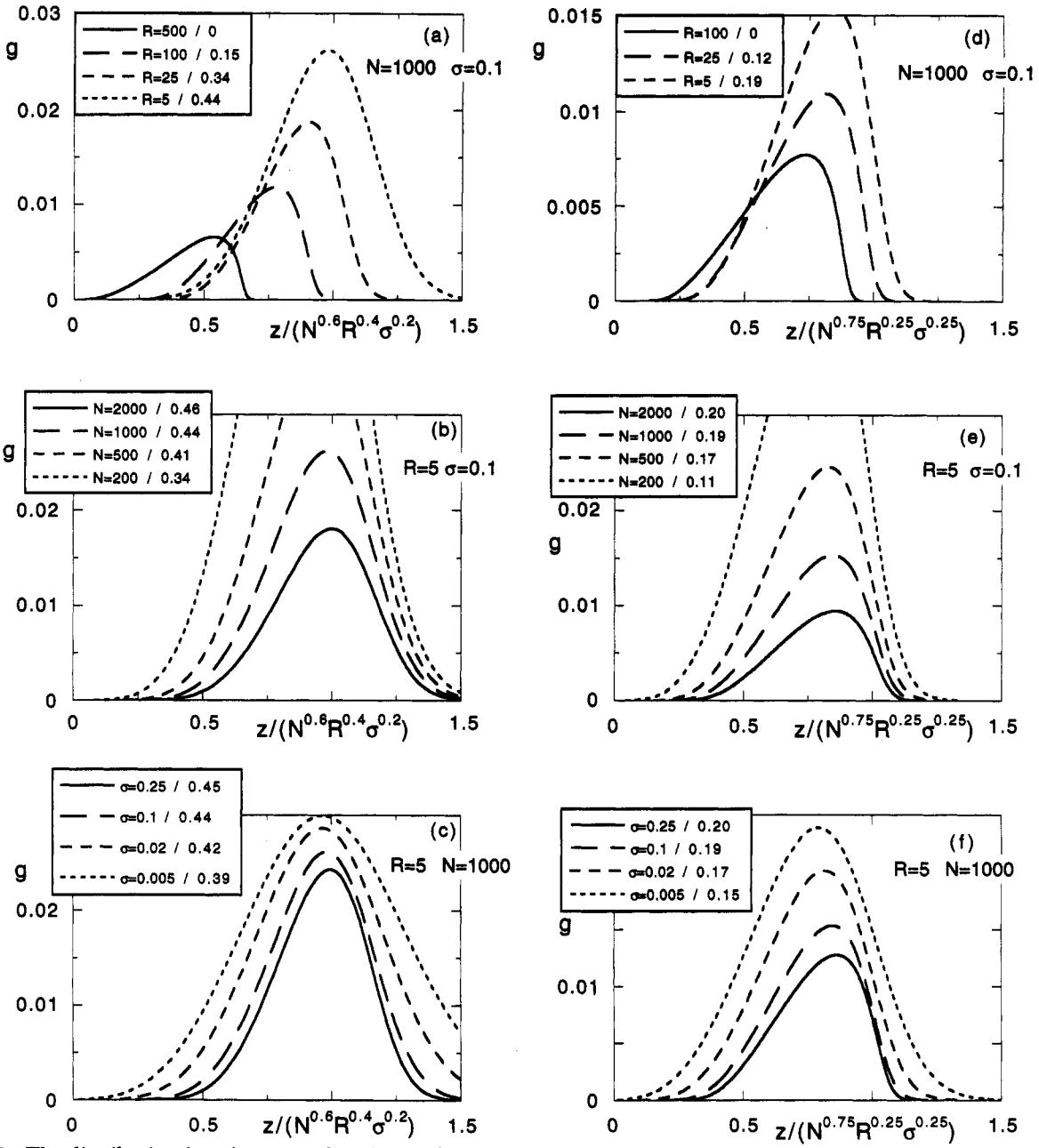

Figure 9. The distribution function g as a function of the normalized distance to the surface in a spherical geometry (a–c) and in a cylindrical geometry (d–f). This distance has been normalized to check the expected scaling behavior of the dead zone: $\Delta \sim N^{3/5}R^{4/5}\sigma^{1/5}$ for a spherical surface, and $\Delta \sim N^{3/4}R^{1/4}\sigma^{1/4}$ for a cylindrical surface. Parameters: R, N, and σ as indicated in the figure; $\chi = 0$. In the legends the numerical values of eq 27 are also given for the indicated set of parameters.

The effect of solvent quality on the free chain end distribution is demonstrated in Figure 10. For solvents varying from good (athermal) to very bad, ($\chi = 1$) $g(z/H_{av})$ has been drawn for a brush on a spherical surface with a high grafting density ($\sigma = 0.1$). Decreasing the solvent quality leads to a collapse of the polymer layer as was seen in Figure 7. However, the distribution of chain ends changes relatively little. Of course the area in which the end segments are located becomes smaller, as the layer height itself becomes smaller, and so the size of the dead zone decreases. The relative size of the dead zone also decreases slightly (as seen from the curve of g versus the reduced distance to the surface, z/H_{av}), but this turns out to be a minor effect.

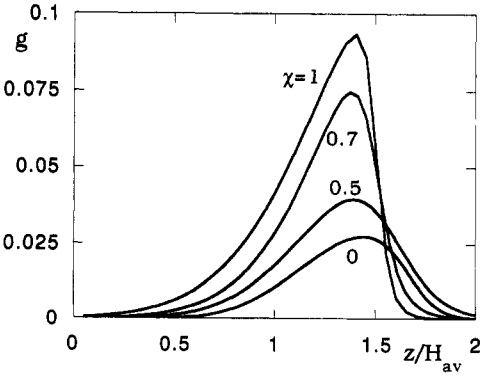

Figure 10. The influence of solvent quality on the chain end distribution. Parameters: $R = 25$, $N = 500$, $\sigma = 0.1$, spherical geometry, $\chi = 0$, 0.5, 0.7, 1.

5. Discussion and Conclusions

In this paper we have shown that the lattice model of the Scheutjens and Fleer theory can be usefully extended to study polymer brushes at spherical and cylindrical interfaces. The efficient method this theory uses to generate chain conformations makes it possible to study the characteristics of polymer brushes over a wide range

of chain lengths (e.g. for far longer chain lengths than is at present possible using simulation techniques). We again emphasize that this theory gives exact solutions within the mean-field theory, in which only nearest-neighbor interactions are accounted for. This makes it an obvious reference point with which to compare approximate analytical SCF descriptions of polymer brushes. We first compared volume fraction profiles with those calculated by Dan and Tirrell.[13] We found good agreement between both models. This is not surprising as both our approaches are based on a very similar physical model.

We have concentrated ourselves on analyzing the volume fraction profiles of brushes at spherical surfaces immersed in an athermal, low molecular weight solvent. For small curvatures the parabolic potential profile model agrees very well with the more accurate lattice calculations. The differences between both descriptions can be largely explained by the fact that the analytical model only takes into account pair interactions between segments. For flat surfaces, differences of the same order of magnitude appear in the volume fraction profile when higher terms are neglected in the mixing free energy of polymer and solvent. Similarly, the distribution of free end segments is roughly the same in both models.

For decreasing radii of curvature, the spurious effect of negative values of $g(z)$ for low z becomes more prominent. As $\int g(z)dz = 1$ this leads to too high values of $g(z)$ outside the dead zone. Furthermore, the lattice calculations predict a finite volume fraction of free chain ends beyond the "classical" chain height. This "foot" of the volume fraction profile can be explained completely analogously to that at the flat interface.[27,33] Increasing the curvature leads to the appearance of a power law-like part in the volume fraction profile.

The "combined model" that we introduced gives a reasonable description of the volume fraction profile by dividing it into two parts. The distribution of free ends in this model is too narrow, but the position of the maximum of this distribution is the same as in the lattice model. For very small particles the lattice model certainly does not indicate that all chain ends are situated at the same height above the surface. The total volume fraction profile for such particles does, however, tend to the scaling law $\phi \sim z^{-4/3}$.

Our lattice calculations show very clear indications of the presence of a dead zone both near spherical and cylindrical interfaces. This is in contradiction with the molecular dynamics results of Murat and Grest,[12] who found no evidence for the existence of a dead zone near a cylindrical surface for any finite radius of curvature. A quantitative comparison of our results with those of Ball *et al.*[11] is not possible, as they solved their SCF equations for a system that we have not considered in this paper, namely a cylindrical brush under melt conditions. Our calculations do, however, suggest that the dead zone size is not a simple monotonic function of the radius. We have tried to explain the radius dependency of the dead zone size in terms of the "combined model" for the volume fraction profile. We hope that our data and this tentative interpretation will encourage further work aimed at better understanding of this dead zone behavior.

In conclusion: we have showed that upon decreasing the solvent quality the grafted layer collapses and forms a step-like profile, irrespective of the curvature. A decrease in solvent quality also leads to a decrease in the dead zone size, but, even for a (far) worse solvent than a Θ-solvent, a dead zone can still exist.

Acknowledgment. We thank Dr. F. A. M. Leermakers and Professer G. J. Fleer for their critical reading of the manuscript. E.B.Z. was supported by The Netherlands Foundation for Chemical Research (SON) with financial aid from The Netherlands Organization for Scientific Research (NWO). E.B.Z. acknowledges the hospitality of Professor Fleer at Wageningen Agricultural University.

References and Notes

(1) Alexander, S. *J. Phys.* (*Paris*) **1977**, *38*, 983.
(2) de Gennes, P. G. *Macromolecules* **1980**, *13*, 1069.
(3) Cosgrove, T.; Heath, T.; Van Lent, B.; Leermakers, F.; Scheutjens, J. *Macromolecules* **1987**, *20*, 1692.
(4) Milner, S. T.; Witten, T. A.; Cates, M. E. *Europhys. Lett.* **1988**, *5*, 413.
(5) Milner, S. T.; Witten, T. A.; Cates, M. E. *Macromolecules* **1988**, *22*, 583.
(6) Zhulina, E. B.; Priamitsyn, V. A.; Borisov, O. V. *Polym. Sci. USSR* **1989**, *31*, 205.
(7) Chakrabarti, A.; Toral, R. *Macromolecules* **1990**, *23*, 2016.
(8) Lai, P. Y.; Binder, K. *J. Chem. Phys.* **1991**, *95*, 9288.
(9) Lai, P. Y.; Zhulina, E. B. *J. Phys. II* **1992**, *3*, 547.
(10) Murat, M.; Grest, G. S. *Macromolecules* **1989**, *22*, 4054.
(11) Ball, R. C.; Marko, J. F.; Milner, S. T.; Witten, T. A. *Macromolecules* **1991**, *24*, 693.
(12) Murat, M.; Grest, G. S. *Macromolecules* **1991**, *24*, 704.
(13) Dan, N.; Tirrell, M. *Macromolecules* **1992**, *25*, 2890.
(14) Daoud, M.; Cotton, J. P. *J. Phys.* (*Paris*) **1982**, *43*, 531.
(15) Birshtein, T. M.; Zhulina, E. B. *Polymer* **1984**, *25*, 25.
(16) Birshtein, T. M.; Borisov, O. V.; Zhulina, E. B.; Khokhlov, A. R.; Yurasova, T. *Polym. Sci. USSR* **1987**, *29*, 1293.
(17) Zhulina, E. B.; Borisov, O. V.; Priamitsyn, V. A. *J. Colloid Interface Sci.* **1990**, *137*, 495.
(18) Semenov, A. N. *Sov. Phys. JETP* **1985**, *61*, 733.
(19) Zhulina, E. B.; Borisov, O. V.; Brombacher, L. *Macromolecules* **1991**, *24*, 4679.
(20) Klushin, L. I.; Skvortsov, A. M. *Macromolecules* **1991**, *24*, 1549.
(21) Grest, G. S.; Kremer, K.; Witten, T. A. *Macromolecules* **1987**, *20*, 1376.
(22) Dolan, A. K.; Edwards, S. F. *Proc. R. Soc. London Ser. A* **1974**, *337*, 509.
(23) Dolan, A. K.; Edwards, S. F. *Proc. R. Soc. London Ser. A* **1975**, *323*, 427.
(24) Scheutjens, J. M. H. M.; Fleer, G. J. *J. Phys. Chem.* **1979**, *83*, 1619.
(25) Scheutjens, J. M. H. M.; Fleer, G. J. *J. Phys. Chem.* **1980**, *84*, 178.
(26) Hirz, S. M.S. Thesis, Univ. of Minnesota 1987.
(27) Wijmans, C. M.; Scheutjens, J. M. H. M.; Zhulina, E. B. *Macromolecules* **1992**, *25*, 2657.
(28) Leermakers, F. A. M.; Scheutjens, J. M. H. M. *J. Phys. Chem.* **1989**, *93*, 7417.
(29) Zhulina, E. B.; Borisov, O. V.; Priamitsyn, V. A.; Birshtein, T. M. *Macromolecules* **1991**, *24*, 140.
(30) Liatskaya, Y. V.; Zhulina, E. B.; Birshtein, T. M. Unpublished results.
(31) Milner, S. T.; Witten, T. A. *J. Phys. Fr.* **1988**, *49*, 1951.
(32) Cohen Stuart, M. A.; Waajen, F. H. W. H.; Cosgrove, T.; Vincent, B.; Crowley, T. L. *Macromolecules* **1984**, *17*, 1825.
(33) Milner, S. T. *J. Chem. Soc. Faraday Trans.* **1990**, *86*, 1349.